Computers in Biology and Medicine 112 (2019) 103377

Contents lists available at ScienceDirect

Computers in Biology and Medicine

journal homepage: www.elsevier.com/locate/compbiomed

Simultaneous localization of multiple tumors from thermogram of tissue phantom by using a novel optimization algorithm inspired by hunting dogs

Seyed Mohammad Salman Lari[a], Afsaneh Mojra[a,*], Mohsen Rokni[b]

[a] Department of Mechanical Engineering, K. N. Toosi University of Technology, 15 Pardis St., Tehran, 1991943344, Iran
[b] Department of Computer Engineering, Shahid Beheshti University, Tehran, Iran

ARTICLE INFO

Keywords:
Thermography
Soft tissue
Early tumor detection
Evolutionary algorithm
Artificial tactile sensing

ABSTRACT

The objective of this study is to couple the contact thermography method with a novel optimization algorithm to rapidly detect and localize the soft tissue tumor. To this end, experiments are carried out on tissue-mimicking phantoms containing resistance heaters to simulate the embedded tumors. An examiner robot is used to measure the temperature of the tissue surface. The time required for the examination of the tissue surface is reduced by developing a novel optimization algorithm called the Hunter Algorithm (HA). In the HA, population individuals are called the hunters, and the global maximum is referred to as the prey. The maximum temperature occurs at the location of the tumor. By the end of the hunting procedure, a flock of hunters converges to the maximum temperature and reaches the tumor while the examination time is significantly reduced. Performance of the HA is evaluated by applying the Genetic Algorithm (GA) and the Particle Swarm Optimization (PSO) algorithm to 11 test functions as minimization problems. It is observed that for the Ackley's function, as an example, the HA finds the global minimum after the 10th iteration with an accuracy of 10^{-4}, while the PSO converges with the same accuracy after the 30th iteration and the accuracy of the GA remains about 0.002. In addition, the results show that the contact thermography in conjunction with the HA is of clinical importance in accurate detection of multiple tumors and small and deeply located tumors with insignificant thermal effects on the tissue surface.

1. Introduction

Constant heat is generated by the human body and is dissipated by a thermoregulatory system [1]. This phenomenon results in the maintenance of the normal body temperature. Disorders and diseases affect the body normal temperature and may increase it up to 2–3 °C. Thermography is a developing non-invasive technique for the diagnosis of diseases which cause an elevation in the body temperature. Thermography provides a map of the body surface temperature, which is referred to as the thermogram [1]. In recent decades, extensive researches have been conducted on the thermography method to determine a close relationship between the body physiology and the temperature of the tissue surface. The success of this technique is verified in the diagnosis of breast cancer [2,3], eye disease [4,5], skin cancer [6,7], joint disease, and bone and thyroid tumors [8,9]. In the presence of a tumor, hot spots can be seen on the thermogram, which is due to a higher surface temperature around the area of cancerous cells compared to the healthy tissue [10]. Thermograms revealed a clear temperature difference up to 3.3 °C, between the tumor core (36.4 °C) and the surrounding healthy tissue (33.1 °C) [11].

Based on the method used for the temperature measurement, thermography can be categorized as contact and infrared. In the infrared (IR) thermography, the infrared energy emitted from an object is detected by an infrared camera or an infrared sensor, and it is converted to apparent temperature on a thermogram [10]. Many types of research have been focused on the ability of the IR thermography in analyzing the physiological condition of the soft tissue. Francis et al. [12] made use of a rotational thermography system for the diagnosis of breast cancer. It was observed that for the healthy breast, there is a continuous temperature band, which could be disturbed by an abnormality. The main drawback of using the IR thermography in their research and similar researches is neglecting the effect of the surface curvature. Since the temperature value depends on the distance between the IR camera/sensor and the tissue surface, neglecting the surface curvature would result in inaccurate estimations. In the IR thermography, the basis of tumor detection is the uniformity disruption in the thermogram; therefore, the difficulty in maintaining similar distance from the IR camera for all points on the surface is a disadvantage of the IR thermography. Shi et al. [13] used the thermal thermography for the diagnosis of skin tumors. In their study, an estimation methodology was

* Corresponding author.
E-mail addresses: smslari@email.kntu.ac.ir (S.M. Salman Lari), mojra@kntu.ac.ir (A. Mojra), mo.rokni@mail.sbu.ac.ir (M. Rokni).

https://doi.org/10.1016/j.compbiomed.2019.103377
Received 26 May 2019; Received in revised form 31 July 2019; Accepted 1 August 2019

presented to determine unknown thermo-physical parameters of a tumor by using the temperature profile on the skin surface. The temperature profile in the tumoral region was interpolated by the bio-heat transfer equation, and the unknown parameters were estimated. The infrared thermography was used as a possible method for obtaining the thermogram. A disadvantage of using the IR thermography in their research and similar researches is the sensitivity of the IR camera/sensor, which limits the functionality of the IR thermography to the superficial layer of the soft tissue. Therefore, small and deeply located tumors, which produce insignificant thermal effects on the tissue surface, would remain undetected. Bahramian et al. [14] proposed an infrared thermal imaging system for the human neck and the thyroid gland. The thermograms were analyzed to distinguish thyroid tumors from the healthy thyroid tissue. The neck curvature and an inadequate accuracy of the IR camera were the main drawbacks of this study. Commonly, to compensate the lack of measurement accuracy, the IR detector is located closer to the object. Unfortunately, the measurement error usually increases by reducing the distance due to the effects of reflectivity and the inclusion of other heat sources within the sensor's field of view.

Contact thermography is used for cancer detection along with the IR thermography. In this method, the temperature is measured by contact temperature sensors on the tissue surface. This method is inspired by the clinical or the physical examination by a physician. Physical examination is the first screening method for early cancer detection. By using a high precision temperature sensor, the accuracy of the contact thermography could be improved. Therefore, regular use of contact thermography could be considered as an inexpensive screening method, which can prevent cancer progression. Contact thermography has been used by Sadeghi et al. [15–17] in recent years for the detection of brain tumors. They have proposed a thermal imaging system for the intraoperative detection of brain tumors. The system was equipped with a contact temperature sensor with a high accuracy. It has been observed that temperature map on the tissue surface is an appropriate outcome of the contact thermography for superficial tumors. Meanwhile, the heat flux map on the surface could be used as an extra thermal result for deeply located tumors. The thermograms were analyzed to localize the brain tumor and identify the tumor margins. The contact thermography has the disadvantage of slow response compared to the IR thermography. However, due to the advantages of higher accuracy in the range of biological temperature and independence from the surface geometrical shape, the contact thermography is preferred and selected in the present study.

In the present study, the contact thermography is employed to detect soft tissue tumor, while the method performance is improved by using the artificial tactile sensing (ATS) method. In the ATS, the tissue surface is slightly compressed during the tissue examination. It has been already affirmed that the tissue compression can improve the quality of thermal measurements, significantly [15]. Therefore, before the temperature measurement, we apply a small compressive strain on the tissue surface. Afterward, the thermogram is constructed by measuring the temperature of different test points on the tissue surface. Tumor detection and localization are carried out by analyzing the thermograms. For accurate tumor detection, several test points should be examined on the tissue surface, which increases the examination time. To overcome this problem, a novel optimization algorithm is introduced to reduce the number of temperature measurements on the tissue surface and to rapidly detect and localize the tumor.

Optimization techniques are extensively used to solve different optimization problems in applied sciences, engineering, industry, biology, and computer science. Some well-known optimization algorithms such as Genetic Algorithm (GA) [18], Particle Swarm Optimization (PSO) [19], Bee Colony Optimization (BCO) [20], Ant Colony Optimization (ACO) [21], Simulated Annealing (SA) [22] and hunting search algorithm [23] are used in this regard. However, these algorithms suffer from significant deficiencies such as the requirement to a large number of input parameters, being unpredictable, producing unripe results and lots of iterations for convergence achievement [24]. Therefore, looking for high-efficiency algorithms is an essential problem in the rapid contact thermography application.

In this regard, a new optimization algorithm is proposed, which is called the Hunter Algorithm (HA) and is inspired by the hunting dogs' behavior. In the HA, all the hunters do their best to hunt the prey on the hunting ground. Following the smell of the prey, leads the hunters to converge to the global maximum on the hunting ground. In this study, the hunting ground, the prey, and the smell are identical to the thermogram, tumor, and the temperature. In addition to improving the rate of convergence, the novelty of the HA is the requirement to only one hunter as the initial population, to find the prey. This is of particular importance in the tumor detection procedure in the contact thermography. In practice, use of one temperature sensor instead of multiple sensors (as the hunters) for scanning the tissue surface would prevent the crosstalk effect on the measured values.

In section 2.2, an experimental setup is described, which mimics the soft tissue containing a tumor. Section 2.3 to section 2.7 explain how the hunting procedure is modeled and implemented among the hunters on the hunting ground. In section 3, the result of rapid tumor detection by the hunting algorithm is provided.

2. Material and methods

2.1. Problem definition

A new optimization algorithm is proposed based on the behavior of hunting dogs, and it is called the Hunter algorithm. At first, the performance of the HA is assessed by the convergence rate and the accuracy of the optimum value for 11 mathematical test functions in comparison to the genetic algorithm and the PSO. In the next stage, a tissue-mimicking phantom made of the agar gel is constructed. The phantom contains a resistance heater, which simulates a tumor with an elevated metabolic activity compared to the healthy tissue. Because of the tumor existence, a temperature gradient appears on the tissue surface. Finding the location of the maximum temperature is a maximization problem that would be solved by the Hunter algorithm. The main purpose of this study is to localize a tumor with a high accuracy and during a short time.

2.2. Examiner robot for thermal measurement

The surface of the soft tissue is examined by an examiner robot (Fig. 1a). The robot mainly consists of three DC motors (24 V, 110 RPM, Buhler 1.61.070.324, Germany) to generate a rotary motion and three perpendicular ball screws (Lead size: 5 mm/round, HIWIN, Taiwan) to convert the rotary motion to a linear motion. It contains three incremental rotary encoders (200 pulses/round) to convert the angular position to a digital code. According to the type of encoders and the ball screws' pitch (5 mm/round), the accuracy of position measurements is 25 μm. The end-effector of the robot can move in a cubic pattern with 400 mm length, 400 mm width and 160 mm height. The probe of the end-effector consists of a contact temperature sensor (SHT 11, Sensirion, Switzerland) for thermal measurements. The temperature sensor measures the temperature in an operating range of -40 °C–123.8 °C with a resolution of 0.01 °C and an accuracy of 0.4 °C. The sensor size is $7.42\ mm \times 4.88\ mm \times 2.5\ mm$ and to examine a surface with dimensions of $100\ mm \times 100\ mm$, approximately 3-h-time is required.

Several in vitro experiments are conducted by the examiner robot on the agar tissue phantoms, which mimic the soft tissue (Fig. 1b). The agar powder is dissolved in water at 1 and 2.0% (water: agar). The mixture is heated up to the boiling point during 2 min with a constant stirring. The agar solution is cooled down in a plexiglass cube with dimensions of $110\ mm \times 60\ mm \times 50\ mm$ at room temperature. Similar to clinical conditions, the room is maintained between 18 and

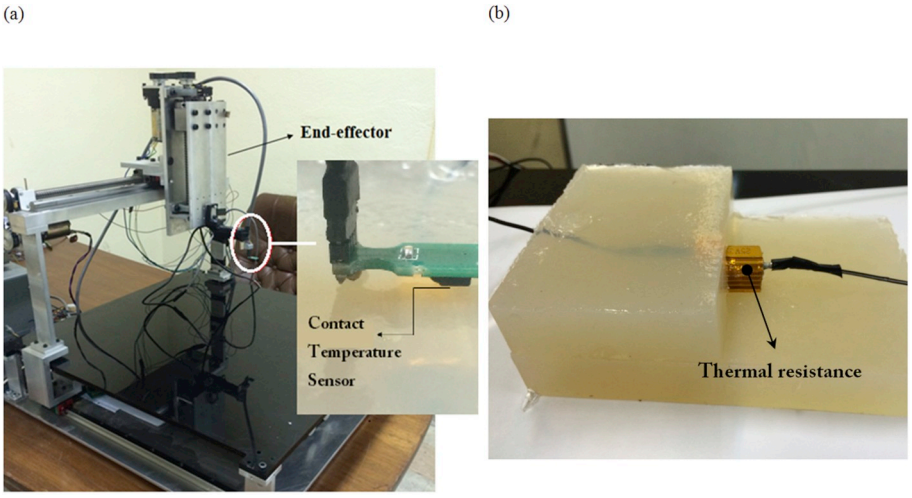

Fig. 1. (a) The examiner robot equipped with a contact temperature sensor, (b) the agar tissue phantom including a resistance heater for mimicking the soft tissue containing a tumor [17].

22 °C while the illumination, sunlight, and humidity of the room are carefully controlled. The agar gel density is 0.99 $\frac{g}{cm^3}$, and the thermal conductivity is 0.55 W/m/K.

To simulate the thermal conditions of the tissue during the physical examination, the cube is insulated with a 2 mm thick natural cork strip on all sides except for the top surface. A 39-Ohm cylindrical resistance heater having 15 mm radius and 25 mm length is used to mimic the embedded tumor. The resistance heater is connected to a 30 V DC power supply to generate 25000 $\frac{W}{m^3}$ heat by the tumor [25].

To detect the tumor, the examiner robot should examine several test points on the tissue surface. To find the spot with maximum temperature, an optimization algorithm called the Hunting algorithm is proposed, to reduce the examination time.

2.3. Hunting algorithm

Hunting is the practice of the killing or trapping an animal by pursuing it. Hunting animals by other animals, which are called predators, is a necessity for their survival [26,27]. Hunting animals by Man is done for the business, or recreation. For such a purpose, dogs are used to find, chase, retrieve, and sometimes to kill the prey. Hunting dogs allow humans to pursue and kill the prey that would otherwise be very difficult or dangerous to hunt. In the Hunting algorithm, the hunting dogs, which are called the hunters, do the action of hunting for trapping the prey. Here, all the hunters compete for taking possession of the prey. In addition, the assimilation policy is considered during the movement of hunters toward the prey.

Fig. 2 shows the flowchart of the Hunting algorithm. Like other evolutionary algorithms, the proposed algorithm starts with an initial population (hunters on the hunting ground), each at a particular location. Subsequently, each hunter begins to take steps along the axes. In every step, the hunter checks the distance to the prey. The critical parameter in the distance measurement is the smell that the hunter feels. By examining the directions, the hunter decides to go along the direction in which the smell is more. By knowing the movement direction, it is time to select the movement pace. In this stage, the proximity to the prey dictates the pace of the movement.

By knowing the direction and the pace of movement, the hunter starts to move. This procedure would be repeated at the new location of each hunter. By the time the hunter is close enough to the prey, the procedure would be terminated. Inattention of getting stuck in the local minima of some functions, hunters may be captured in traps (local minima) which have been located on the hunting ground, and the hunters can no longer continue to hunt. This issue is dissolved by employing multiple hunters that try to reach the prey. Unlike conventional evolutionary and swarm intelligence-based algorithms, the HA could be carried out by one hunter as the initial population to find the prey.

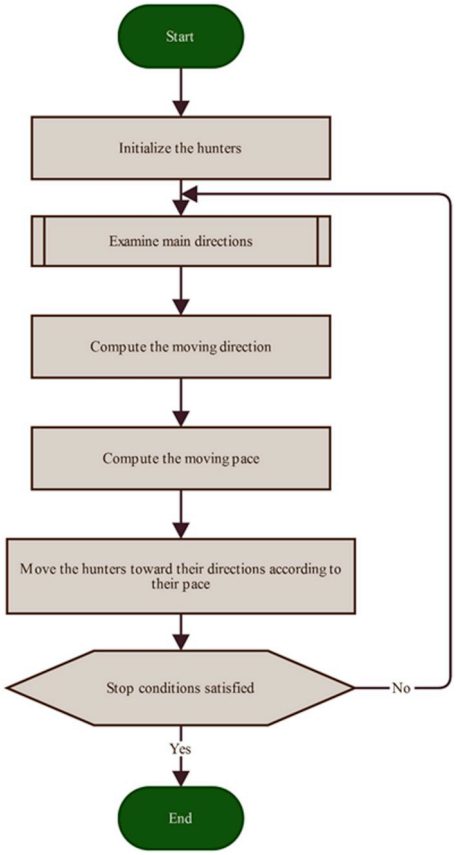

Fig. 2. Flowchart of the Hunter optimization algorithm.

2.4. Generation of initial hunters

The goal of optimization is to find an optimal solution, which is the maximum temperature, in terms of the variables of the problem. The variables are the temperature values at different test points. Each variable is referred to as a hunter. The hunter is identical to the

chromosome in the GA terminology. Each hunter is an $1 \times N_{var}$ array and is defined by Eq. (1):

$$h = [p_1, p_2, p_3, ..., p_{N_{var}}] \quad (1)$$

Where h is the hunter and $p_i s$ are the coordinates of each hunter. For the two-dimensional movement of the hunter, p_1 and p_2 are x and y in the Cartesian coordinate system, respectively. The cost function (f), is defined for each hunter by Eq. (2):

$$cost = f(h) = f(p_1, p_2, p_3, ..., p_{N_{var}}) \quad (2)$$

To start the optimization algorithm, an initial population of size N_{hunter} is generated. The hunters are distributed randomly on the hunting ground.

2.5. Examine main directions

Each hunter with N-dimensional coordinate system has $2N$ options for the direction of the next movement. The hunter takes one-step forward and backward along each axis, according to Eq. (3).

$$h_i^{\pm} = [p_1, p_2, p_3, ..., p_i \pm step, ..., p_N] \quad (3)$$

Where, is the step of movement in p_i - direction. Fig. 3a shows four main directions along p_1 and p_2 axes for the 2D movement of a hunter.

By moving one-step along each of four directions, the smell of the prey is sensed and memorized by the hunter. The recorded smells in the ith-direction are presented by Eq. (4).

$$S_i^{\pm} = \frac{1}{f(h_i^{\pm})} \quad (4)$$

Where S_i is the smell or the temperature at $h_i^{\pm}$. The function S_i is defined as a new cost function to solve a maximization problem and obtain the maximum temperature instead of the minimization of the function $f(h_i)$, which has been previously defined by Eq. (2).

Eq. (4) could be improved by increasing the step of movement ($step$) by adding a specific amount, which is referred to as the virtual step (ε). Therefore, the smell can be measured at the new step by Eq. (5):

$$S_i^{\pm} = \frac{\varepsilon}{|f(p_1, p_2, p_3, ..., p_i \pm step + \varepsilon, ..., p_N) - f(h_i^{\pm})|} \quad (5)$$

By using Eq. (5) instead of Eq. (4), the time required for reaching the prey is reduced. However, the accuracy of hunting may be attenuated. To reduce the hunting time while maintaining the hunting accuracy, half of the hunters are treated by the first method through Eq. (4) and the rest of hunters by the second method, through Eq. (5).

To define the new location of the hunter, the smell values in Eq. (4) should be compared. According to the smell values, the hunter moves in the direction with a higher smell. The step to the prey in the ith-direction is defined by Eq. (6):

$$d_i = Max(S_i^-, S_i^+) \quad (6)$$

In fact, every hunter is looking for a high smell around itself and wants to move towards the prey with the minimum pace. Hunters are trained to be aware that moving in wrong directions will lead to high costs. The pseudo-code of the HA in examining main directions is provided in Fig. 3b.

2.6. Compute the movement direction and pace

By checking the main axes, the hunter selects between the positive and the negative directions on each axis based on higher smell values. The final movement direction is a resultant vector among the directions chosen on each of the main axes. Each direction has a weighted contribution in the resultant movement vector according to the smell values. In fact, every step to the prey along the ith-direction (has been defined by Eq. (6)) is rated by the hunter and has a particular weight

(a)

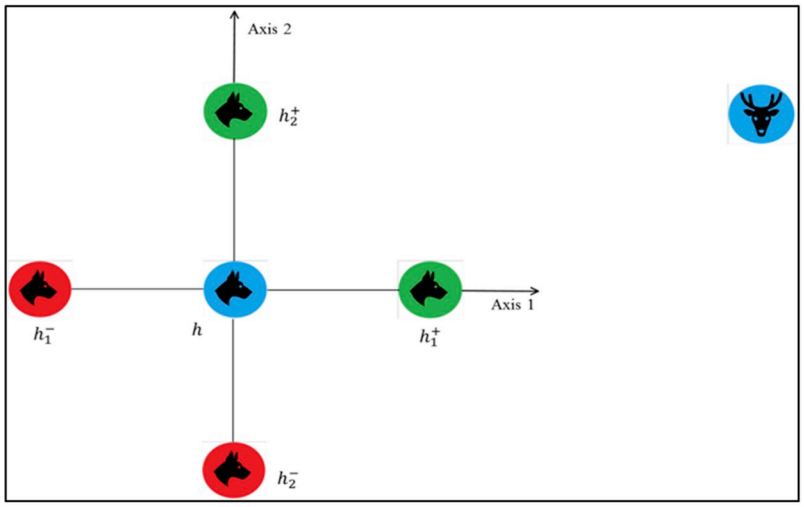

(b)

```
for each dimension i = 1, …, n do
      take one step forward and backward for all hunters: h+ and h-
      compute the smell function for new positons: S(h+) and S(h-)
      if S(h+) > S(h-) then
            choose best dimension as the positive step: d = S(h+)
      else
            choose best dimension as the negative step: d = S(h-)
```

Fig. 3. (a) The schematic and (b) the pseudo-code of examining main directions by the hunter for a 2D movement.

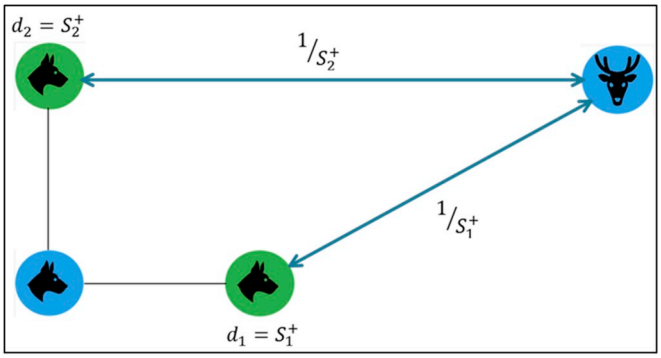

Fig. 4. The schematic of weighting each direction by the hunter toward the prey in a 2D movement.

compared to other steps in other directions. In Fig. 4, the schematic of weighting by the hunter is displayed.

To determine the weights, Eq. (7) to Eq. (9) are used:

$$t = \sum_{i=1}^{N} d_i \tag{7}$$

$$w_i(+\,dir.\,) = \frac{S_i^+}{t} \times step \tag{8}$$

$$w_i(-\,dir.\,) = \frac{S_i^-}{t} \times step \tag{9}$$

where, w_i is the weight of steps in each direction.

Now, these weights come to the form of a vector, and the components are normalized by the square root of the sum of squares of all weights, given by Eq. (10).

$$D = \frac{[w_1, w_2, w_3, \ldots, w_N]}{\sqrt{\sum_{i=1}^{N} w_i^2}} \tag{10}$$

Where, D is the normalized movement vector for each hunter. This vector is presented in Fig. 5a, and the related pseudo-code is provided in Fig. 5b.

By knowing the normalized movement vector (D), the hunter takes one step and records the smell of the prey at the new location which is $S(h + D)$ (Fig. 6a). Afterward, the hunter compares this value with the corresponding value at the previous location, which has been indicated by $S(h)$. According to the smell ratio at the new and the previous locations, the pace of movement is defined by Eq. (11).

$$P = \begin{cases} \frac{S(h+D)}{S(h)}, & S(h) \geq S(h+D) \\ \frac{S(h)}{S(h+D)}, & S(h) < S(h+D) \end{cases} \tag{11}$$

P is the pace of movement and is always smaller than unity. The pace of movement helps to control the distance between the new and the previous locations of the hunter. The pseudo-code of finding the pace of movement is provided in Fig. 6b.

In case of dealing with a hunting ground with fewer traps or local minima, the following equation is suggested for the movement pace:

$$P = \frac{\sum_{i=1}^{N} |f(p_1 + e_1, p_2 + e_2, p_3 + e_3, \ldots, p_i + e_i + \varepsilon, \ldots, p_N + e_N) - f(h + e)|}{\sum_{i=1}^{N} |f(p_1, p_2, p_3, \ldots, p_i + \varepsilon, \ldots, p_N) - f(h)|} \tag{12}$$

where, $f = \frac{1}{S}$ according to Eq. (4).

By identifying the movement direction and the pace, it is time for the hunter to move. The movement vector is defined by multiplying the direction vector by the pace of movement, as presented by Eq. (13).

$$\vec{m} = P\vec{D} \tag{13}$$

Therefore, the new location of the hunter can be defined by Eq. (14) as follows:

$$h_{new} = h + m \tag{14}$$

Fig. 7a shows the hunter at its new location. The pseudo-code of the hunter movement to the new location is provided in Fig. 7b.

(a)

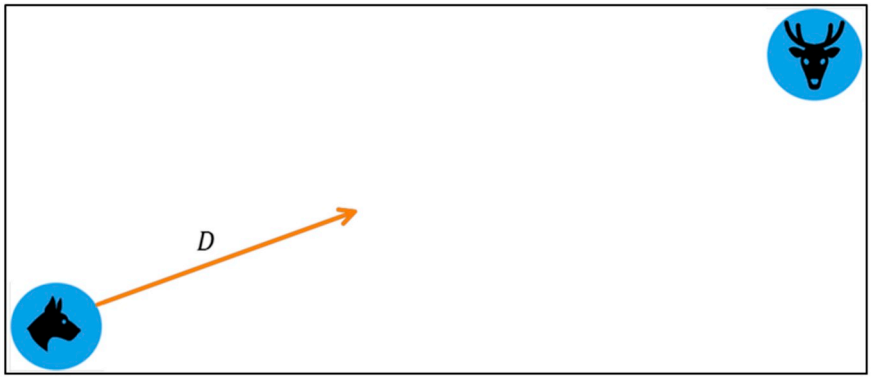

(b)

```
initialize the sum of best dimensions: t = 0
for each dimension i = 1, …, n do
      compute the sum of best dimensions: t = t + d
for each dimension i = 1, …, n do
      if d = S(h+) then
            compute the weight by using the step value: w = (S(h+) / t) * s
      else
            compute the weight by using the step value: w = (S(h-) / t) * (-s)
      compute the direction: D = w / length(w)
```

Fig. 5. (a) The schematic and (b) the pseudo-code of computing the normalized movement vector for each hunter in a 2D movement.

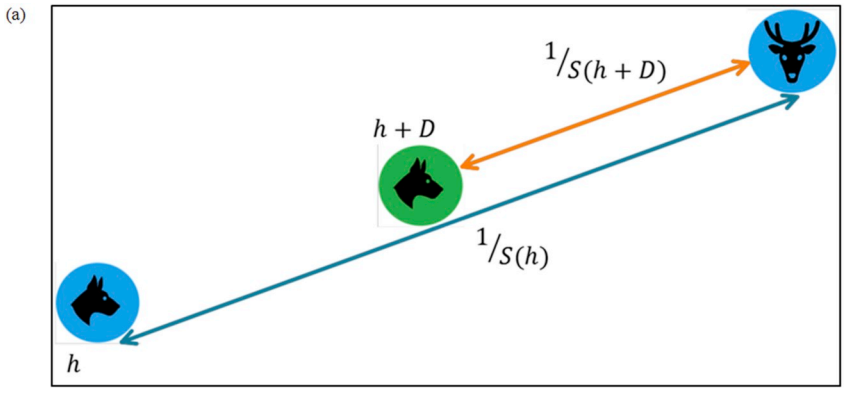

Fig. 6. (a) The schematic of comparing the smell at the new hunter location with the smell at the previous location, (b) the pseudo-code of computing the pace of movement according to the smells at the new and the previous hunter locations.

2.7. Stopping criteria

There are a large number of hunters on the hunting ground, and each hunter tries to reach the prey through the Hunting algorithm. Such hunting has the benefit that the hunters do not necessarily have the same location during the hunting procedure. Each hunter has a particular cost, according to Eq. (4) and the procedure would be terminated by evaluating the minimum cost among the hunters.

There are two stopping criteria for the proposed algorithm. The algorithm can be terminated either by limiting the number of iterations or by reaching a sufficiently small error value. The error (ε) is the difference between the function's values in two consequent iterations (Eq. (15)).

$$\varepsilon = f(h_{new}) - f(h) \tag{15}$$

3. Results

The performance of the Hunter algorithm is initially tested by the Ackley's function in a minimization problem. Properties of this function and the optimization domain are presented in Table 1.

Although the HA could be carried out by one hunter on the hunting ground, an initial population of 100 hunters is selected and shown in Fig. 8. The multiplicity of hunters can provide the possibility of comparing the performance of the HA with other evolutionary and optimization algorithms. Each hunter shown by " × " mark is looking for the minimum value, individually. Fig. 8a, b, 8c, and 8d show the hunters distribution at the initial stage, and after the 17th, 34th, and 50th iterations, respectively. It can be seen that at the 17th iteration, some of the hunters are at the local minima and some of them are searching for the global minimum of the function. At the 34th iteration, only 48 hunters are trapped. At the 50th iteration, few hunters are trapped, and the flock of hunters (67 hunters) has almost reached the prey. The minimum converged value by the hunters is 2.8422×10^{-15} at this iteration. This problem has also been studied by the genetic algorithm, and it has been observed that at the 50th iteration, the converged value is 3.9096×10^{-3}, which is higher by 12 orders of magnitude in comparison with the achievement of the Hunter algorithm.

The performance of the HA is evaluated by applying the GA and the PSO to this problem. To make a comparison among these methods, the initial population of 100 is selected for all of the optimization methods. In the continuous GA, mutation and selection rates are set to 0.3 and

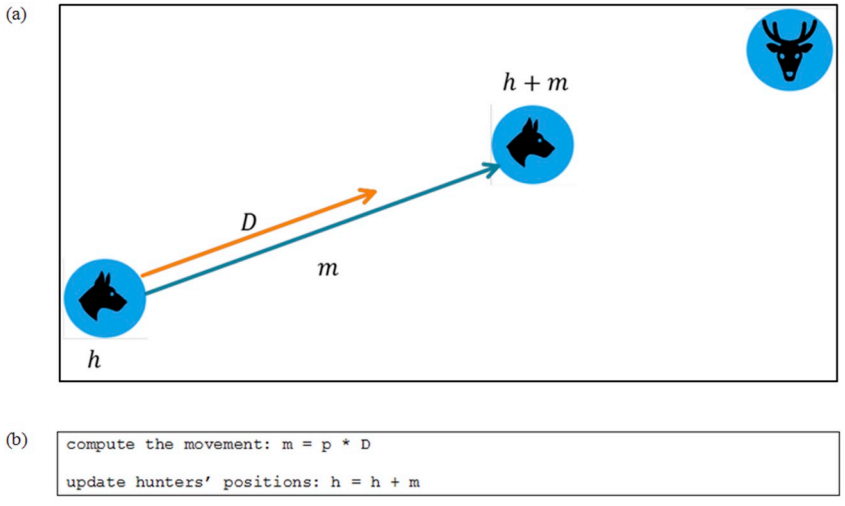

Fig. 7. (a) The schematic of the new hunter location, (b) the pseudo-code of computing the movement vector for a hunter in a 2D movement.

Table 1
Properties of the Ackley's function for a minimization problem, the plot is obtained from https://en.wikipedia.org/wiki.

Plot	Formula [28]	Minimum	Search Domain
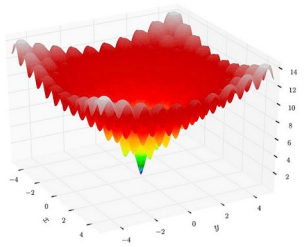	$f_1(x, y) = -20\exp(-0.2\sqrt{0.5(x^2 + y^2)}) - \exp(0.5(\cos(2\pi x) + \cos(2\pi y)))+ e + 20$	$f_1(0,0) = 0$	$\lvert x\rvert < 5,$ $\lvert y\rvert < 5$

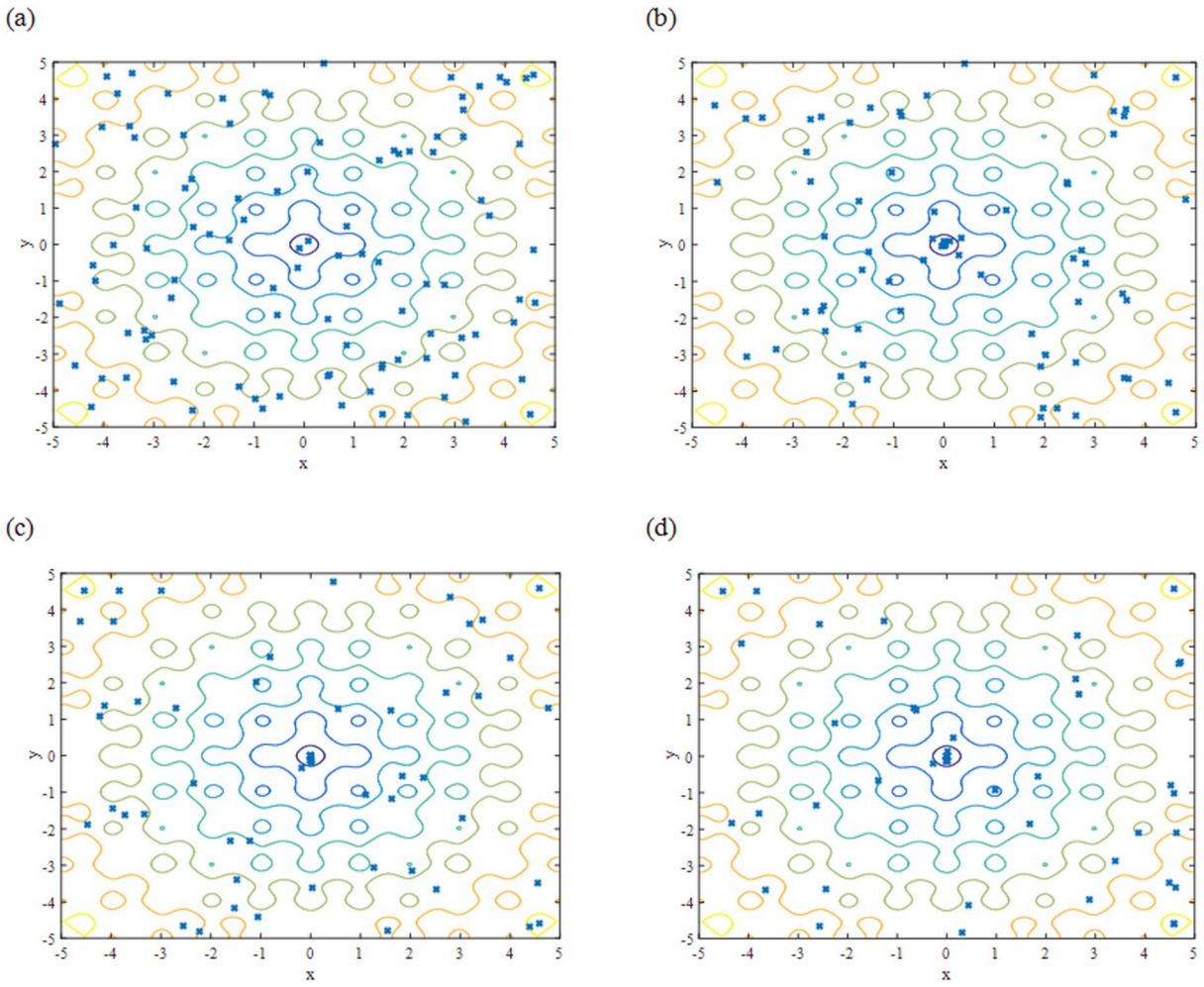

Fig. 8. The distribution of 100 hunters on the hunting ground for finding the global minimum of the Ackley's function at (a) the initial stage, and after (b) the 17th iteration, (c) the 34th iteration, and (d) the 50th iteration.

0.5, respectively, and for the PSO, p-increment and g-increment parameters are set to 2. The minimum cost of population versus generation is displayed in Fig. 9. It could be inferred from this figure that at the 10th iteration, the HA finds the minimum with a difference less than 0.0001, whereas the PSO converges to the global minimum with this accuracy at the 31st iteration, and the GA does not attain such accuracy.

The performance of the Hunter algorithm is tested by ten other well-known minimization problems. The numbers of initial hunters and the number of iterations used in the problem f_2 to f_{11} are 100 and 50, respectively. Details of the functions and comparison between the optimum values obtained by the HA and the GA, are provided in Table 2. According to this table, the minimum value for problems f_2 –f_4 and f_6 –f_9 is equal to zero. Optimum values acquired from the GA are up to 10, 3, 710, 550, 17, 21 and 36 times greater than the corresponding values by the HA.

The Hunter algorithm is employed to detect soft tissue tumors based on thermal measurements on the tissue surface. Fig. 10 is the thermogram on the agar surface, which is a 3D plot of the surface temperature obtained by the examiner robot. The maximum temperature on the interval $0 < (x \ \& \ y) < 100\ mm$ is located at $(50\ mm, 50\ mm)$, in the center of the tissue sample, and it is equal to 40 °C. Appearance of the peak is due to the existence of the tumor.

Several in vitro experiments are carried out by the examiner robot

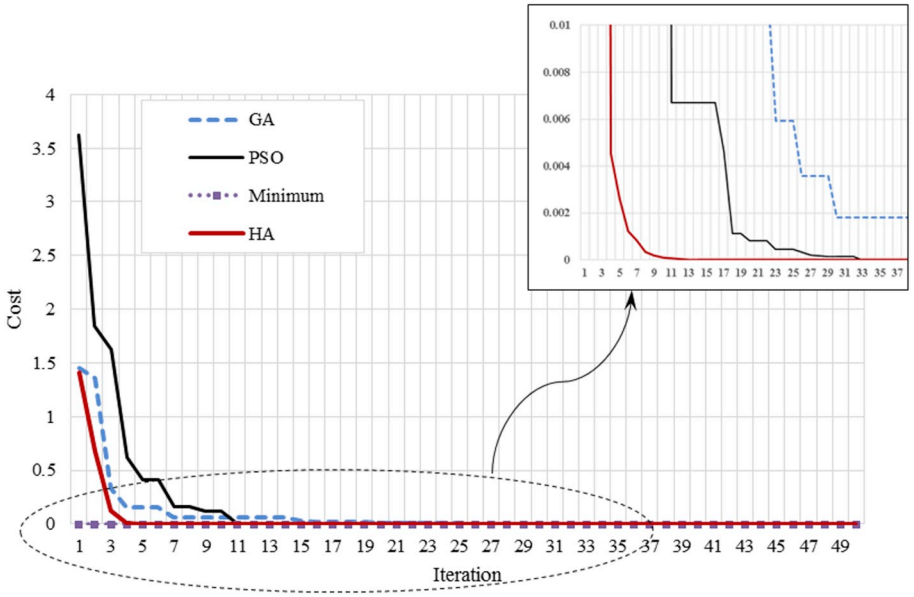

Fig. 9. Comparison of minimum costs of the problem f_1 by the HA, GA, and the PSO versus iteration (convergence rate).

according to Table 3. Considering a constant power and location for the resistance heater in all experiments except for cases P_{10} and P_{11}, a maximum temperature of 40 °C is observed. In the last experiment (P_{11}), the location of the resistance heater is changed in depth. By getting far from the surface, the maximum temperature decreases, as could be inferred from Table 3.

Following the experiments, 11 optimization problems are defined to be solved by the proposed Hunter algorithm. The objective is to find the maximum temperature and its location while minimizing the number of measurements on the surface. By doing this, the time required for tumor detection would also be minimized. In the following, problems P_1, P_2, P_6 and P_{10} are studied in details. The rest of the results are provided in brief.

The Hunter algorithm starts with an initial population of 1 hunter looking for the point with maximum smell or temperature. Details of the HA properties are presented in Table 4.

The hunter is shown by a hollow square (□) in Figs. 11 and 12. Fig. 11a, b, and 11c, and Fig. 12 show the hunter movement in problems P_1, P_2, P_6 and P_{10}, respectively. From the grid in Fig. 10a, the hunter starts from the point located at (3 mm, 95 mm), while the prey is located in the middle of the hunting ground. The pace of movement is bigger at the beginning of the hunting procedure when the hunter is far from the prey. By getting closer to the prey, the pace is reduced. In Fig. 11a, the sequence of iterations indicates a larger distance between the hunter's locations during the initial iterations compared to the latter ones. If the initial location of the hunter becomes closer to the prey, as could be seen in problem P_6, the number of iterations and the run time of the hunting procedure are reduced.

In problem P_2, the initial location of the hunter is close to the prey; therefore, the movement pace is selected accurately, and it is small, and the prey is hunted after a few iterations (Fig. 11b).

For deeply located tumors, including the case in problem P_{10}, the temperature gradients are decreased. Therefore, it would be more difficult to hunt the prey. To detect the prey, the pace of movement should be selected cautiously. As can be seen in Fig. 12, the paces are considerably smaller than those in problems P_1 and P_6. If the hunter starts from similar points on the hunting ground, more iterations are required for deeply located tumors.

The temperature versus iteration is plotted in Fig. 13 for the problems P_1, P_2, P_6 and P_{10}. Increase of the number of iterations indicates that a longer time is required for tumor detection and localization.

Details of 11 optimization problems with data related to the Hunter algorithm application are provided in Table 5. As it has been previously mentioned, the time required to examine a surface with dimensions of 100 $mm \times 100$ mm is approximately 3 h or 10,800 s. Table 5 shows that even if the start point of the hunter is at the furthermost point of the hunting ground, only a few seconds are required to localize the tumor. In this case, in regions with minor temperature gradients, the hunter moves faster with larger steps. By getting close to the prey, the movement step becomes smaller and it takes more iterations for the hunter to reach the tumor. The hunter movement toward the prey, when the initial location of the hunter is at the farthest point from the prey, could be observed in Figs. 11a and 12.

It should be mentioned that for problems p_1 to p_{11}, the thermograms are plotted just for a better understanding of the hunter movement toward the tumor, i.e., by using the HA, the hunter moves toward the tumor without any awareness of the pattern of the temperature profile. Therefore, the thermal map is not constructed before the employment of the Hunter algorithm. In fact, the measurement by the examiner robot is performed for some selected test points picked by the HA. This would result in the development of a non-continuous and sparse thermogram on the tissue surface. Construction of the HA-based thermogram requires a short time.

The Hunter algorithm is tested on tissue thermograms with multiple tumors. Thermograms of tissue with two embedded tumors and tissue with three tumors are displayed in Fig. 14a and c. As could be seen, there are significant differences between the peaks in both thermograms. The first peak occurs at the location of (50,70) and is related to a rather superficial and large tumor. The second tumor is located at (70,40) in Fig. 14a and is located at (60,50) in Fig. 14c. The second peak is related to a medium-sized tumor, whereas the third peak in Fig. 14c is related to a small-sized or a deeply located tumor. The normal temperature in Fig. 14a is 35 °C, and temperature elevation is up to 7% and 4.5% for the first and second tumors, respectively. According to Fig. 14c, the normal temperature is 37.5 °C, and temperature rise for the three tumors is approximately 4.5%, 3%, and 1%. 1% temperature rise is very low concerning the detectable temperature rise by conventional thermography methods. Figs. 14b and d shows the movement of hunters toward the tumors. Both thermograms are marched with a random initial location of the hunters. With regard to Fig. 14b, the first and second tumors are detected after the 12th and 13th iterations. For the thermogram with three peaks, the first and

Table 2
Details of mathematical functions and comparison of the HA and the GA by the accuracy of the optimum values, plots are obtained from https://en.wikipedia.org/wiki.

Function Name	3D Plot	Function Formula	Minimum value	Search Domain	Optimum value of the cost function	
					GA	HA
Sphere function [28]	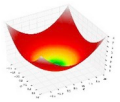	$f_2(x,y) = x^2 + y^2$	$f_2(0,0) = 0$	$-\infty < x, y < \infty$	2.5002×10^{-3}	2.6145×10^{-4}
Rosenbrock function [28]	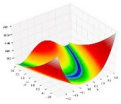	$f_3(x,y) = 100(y - x^2)^2 + (x-1)^2$	$f_3(1,1) = 0$	$-\infty < x, y < \infty$	2.8738	1.0521
Beale function [28]	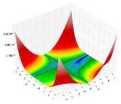	$f_4(x,y) = (1.5 - x + xy)^2 + (2.25 - x + xy^2)^2 + (2.625 - x + xy^3)^2$	$f_4(3,0.5) = 0$	$-4.5 < x, y < 4.5$	5.2628×10^{-1}	7.4030×10^{-4}
Goldstein–Price function [28]	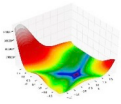	$f_5(x,y) = \left(1 + (x+y+1)^2 \left(19 - 14x + 3x^2 - 14y + 6xy + 3y^2\right)\right) \times \left(30 + (2x-3y)^2 \left(18 - 32x + 12x^2 + 48y - 36xy + 27y^2\right)\right)$	$f_5(0,-1) = 3$	$-2 < x, y < 2$	3.0029	3.0215
Booth function [28]	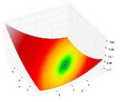	$f_6(x,y) = (x + 2y - 7)^2 + (2x + y - 5)^2$	$f_6(1,3) = 0$	$-10 < x, y < 10$	7.6235×10^{-4}	1.3889×10^{-6}
Matyas function [28]	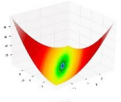	$f_7(x,y) = 0.26(x^2 + y^2) - 0.48xy$	$f_7(0,0) = 0$	$-10 < x, y < 10$	2.3056×10^{-5}	1.3573×10^{-6}
Levy function [28]	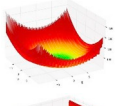	$f_8(x,y) = \sin^2(3\pi x) + (x-1)^2(1 + \sin^2(3\pi y)) + (y-1)^2(1 + \sin^2(2\pi y))$	$f_8(1,1) = 0$	$-10 < x, y < 10$	3.3600×10^{-4}	1.5953×10^{-5}
Three-hump camel function [28]	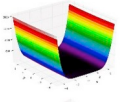	$f_9(x,y) = 2x^2 - 1.05x^4 + \frac{x^6}{6} + xy + y^2$	$f_9(0,0) = 0$	$-5 < x, y < 5$	8.1648×10^{-6}	2.2546×10^{-7}
Cross-in-Tray function [28]	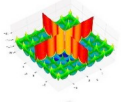	$f_{10}(x,y) = -0.0001(\lvert \sin(x)\sin(y) \exp\left(\left\lvert 100 - \frac{\sqrt{x^2+y^2}}{\pi}\right\rvert\right)\rvert + 1)^{0.1}$	$f_{10}\begin{pmatrix}1.64941,\\ -1.34941\end{pmatrix} = -2.06261$	$-10 < x, y < 10$	-2.0626	-2.0626
Eggholder function [28]	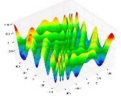	$f_{11}(x,y) = -(y+47)\times \sin\left(\sqrt{\left\lvert y + \frac{x}{2} + 47\right\rvert}\right) - x\sin(\sqrt{\lvert x - (y+47)\rvert})$	$f_{11}\begin{pmatrix}512,\\ 404.2319\end{pmatrix} = -959.6407$	$-512 < x, y < 512$	-9.2536×10^{2}	-9.3241×10^{2}

second tumors are found after the 9th and the 11th iterations, while the smallest peak is detected after the 17th iterations. Increased number of iterations for the third tumor is related to the minor thermal effects on the thermogram compared to two other tumors.

The Hunter algorithm is also applied to the thermograms obtained by Dua et al. [29] and Mulaveesala et al. [30]. In these studies, an infrared camera was used to detect radiations from the surface of the breast tissue and to map the thermal gradients on a thermogram. Linear frequency modulated thermal wave imaging was adopted to detect tumors of the breast. Results were indicative of the presence of 4 tumors. Table 6 presents the number of iterations by using the Hunter algorithm to detect and localize all embedded tumors. Performance of the hunter algorithm could be evaluated by investigation of the difference between the exact and the optimum values of the temperature and the location of the embedded tumors. It is clear that the HA can rapidly and precisely detect and localize the breast tumors.

Considering the results presented above, the Hunter algorithm has two significant privileges compared to conventional evolutionary and optimization algorithms. First, by employing the HA, the accuracy of the optimum value, and the rate of convergence are significantly improved compared to the GA and the PSO. Results provided in Table 1, Fig. 9, and Table 2 state that by fixing the population size for the HA, GA and the PSO, the accuracy could be improved up to 12 orders of magnitude; meanwhile, the number of iterations is reduced. In order to compare the performance of the HA with recently developed optimization algorithms, the Cuckoo search algorithm is selected, and the population size is fixed. The Cuckoo search (CSCo) is one of the nature-inspired algorithms, which has been used extensively for optimization problems in different fields of engineering. This algorithm was improved by Marelia and Twala [31], and three new Cuckoo search

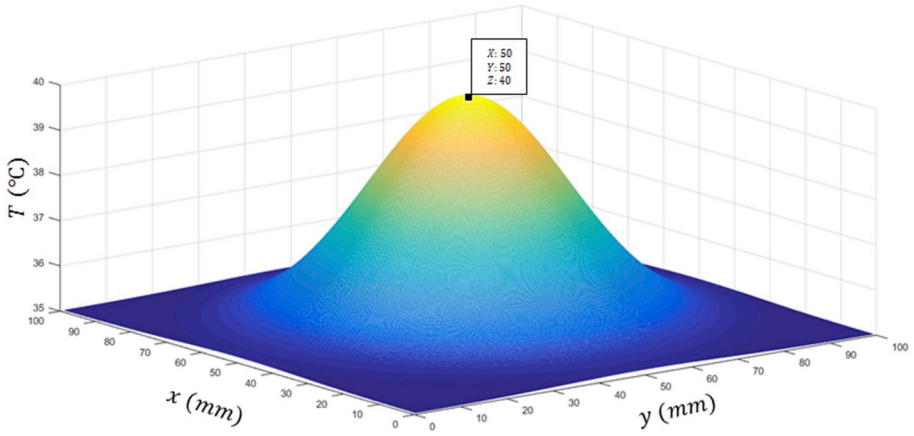

Fig. 10. Plot of the thermogram on the agar surface with dimensions of 100 mm × 100 mm containing a tumor in the central point.

Table 3
The tumor location and the maximum temperature obtained from different in vitro experiments conducted on the agar samples by the examiner robot.

Case Number	Tumor Location (mm)	Maximum Temperature (°C)
P_1	(50,50)	40
P_2	(8,90)	40
P_3	(87,85)	40
P_4	(82,20)	40
P_5	(23,25)	40
P_6	(50,50)	40
P_7	(50,50)	40
P_8	(50,50)	40
P_9	(50,50)	40
P_{10}	(50,50)	40
P_{11}	(50,50)	37.5

Table 4
Details of the Hunter algorithm in problems P_1 to. P_{11}.

Parameter	Value
Problem dimension	2
Iteration limit	50
Number of hunters	1
Step (s)	1 mm

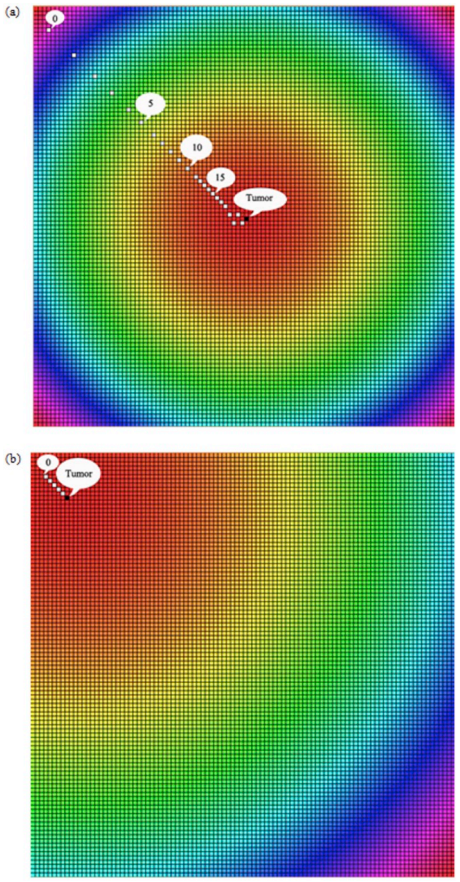

Fig. 11. The hunter movement toward the prey in problems (a) P_1, and (b). P_2.

algorithms were introduced based on dynamically changing switching parameters. These algorithms were referred to as CSLD (the Cuckoo search using linear decreasing switching parameter), CSLI (the Cuckoo search using linear increasing switching parameter), and CSEI (the Cuckoo search using exponential increasing switching parameter). The three algorithms, along with the CSCo were tested on a number of mathematical test functions. Results of this study showed that for the Ackley test function, as an example, the global minimum is 1.10×10^{-7} by the CSCo, 9.67×10^{-8} by the CSLD, 3.35×10^{-8} by the CDLI, and 5.94×10^{-7} by the CSEI, while it is 2.8422×10^{-15} by the Hunter algorithm. This comparison shows that the HA is much more exact than the Cuckoo search algorithm and its derivatives. The Rain-fall algorithm (RFO) is another optimization algorithm which was proposed by Kaboli et al. [32] based on the behavior of raindrops. It was declared that the RFO is unaffected by the parameter setting of the applied optimization method. The RFO result for the minimization of the Ackley function was reported to be 1.724×10^{-4} which is less accurate than the result by the HA, by orders of magnitude. Moreover, the Bat algorithm (BAT) [33,34] and the Firefly algorithm (FF) [34,35] were employed for assessment of the HA while the population size is fixed for the sake of equality (n = 50). It was observed that the optimum value at the 30th iteration is 2.3629 by the BAT and 8.1779×10^{-5} by the FF for the Ackley function, while it is 2.5821×10^{-10} by the HA. For the Eggholder function, the optimum value is −831.837 by the BAT and −816.391 by the FF, while it is −923.344 by the Hunter algorithm. In addition to the better performance of the HA in the optimization process, another privilege of the HA is that unlike most of the optimization and evolutionary algorithms, the HA is not disturbed by the determination of the number of the initial population. In fact, the Hunter algorithm is not swarm intelligence-based algorithm and could be carried out by only one hunter as the initial population to find the prey. The large number of the initial population, which is required for many optimization algorithms, has many disadvantages including the need for parallel implementation, rather slow convergence, and long search time. In addition, the setting

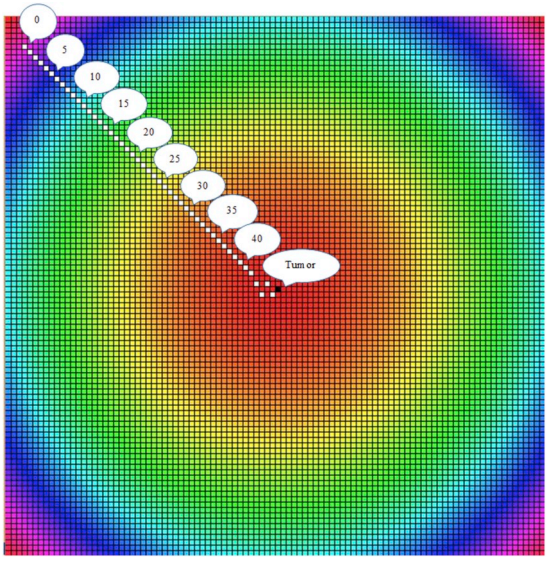

Fig. 12. The hunter movement toward the prey in the problem. P_{10}.

of various parameters is determined by the experience; therefore, it has a high dependence on the specific application [36]. Significance of the HA is not limited to the optimization strategies. The HA is of clinical importance in simultaneous localization of multiple tumors from the 2D thermogram with multiple local extrema. Furthermore, the HA could detect an insignificant temperature gradient on the thermal map, which could be related to a small tumor or a deeply located tumor.

4. Discussion

In the present study, the contact thermography is used for the detection and localization of soft tissue tumors. The soft tissue is mimicked by the agar gel, and a resistance heater is placed within the sample for mimicking the tumor. An examiner robot is employed to measure the surface temperature by a contact temperature sensor. It is estimated that for the construction of a thermogram, which includes all points on the tissue surface, a couple of hours are required. To reduce the examination time without affecting the accuracy of the diagnosis procedure, a new optimization algorithm is developed. The algorithm is named the Hunter algorithm since it is inspired by the behavior of dogs in hunting the prey. The critical parameter in the Hunting algorithm is the smell that the hunter feels. By examining the directions, the hunter decides to go in the direction in which the smell is more. By the time the hunter is close enough to the prey, the procedure would be terminated.

Table 5
Number of iterations and the time required to reach the point with the maximum temperature for different cases presented in Table 3.

Problem	Start Point (mm)	Iteration	Time (sec)
P_1	(3,95)	22	24
P_2	(3,95)	4	4
P_3	(3,95)	33	36
P_4	(3,95)	25	27
P_5	(3,95)	32	35
P_6	(8,90)	21	23
P_7	(8,90)	20	22
P_8	(82,20)	19	21
P_9	(23,25)	18	19
P_{10}	(3,95)	46	50
P_{11}	(3,95)	46	50

In order to evaluate the performance of the HA, minimum values of 11 mathematical test functions are calculated by employing the HA. According to Table 2, multiple and large numbers of global minima and the convex shape are the main characteristics of the selected test functions. Results in Table 2 and Fig. 9 specify that the performance of the Hunter algorithm is improved compared to the GA and the PSO by the convergence rate. Meanwhile, the accuracy of the optimum value by the HA is increased by orders of magnitude for an identical number of the initial population and iterations.

However, the motivation of the work is not only limited to the optimization of intricate mathematical functions, but also the proposed algorithm is developed with a clinical significance in improving tumor detection and localization procedures. It is desirable to detect tumors at early stages when the tumor size is small, and the chance of a successful treatment is high. The thermography method could be employed for the tumor detection because cancerous cells generate more heat than normal cells due to their higher metabolic activity, their angiogenesis, and their vascular dilation [37]. However, the thermography application is limited by the tumor size. For tumor cases with a high amount of heat generation and a high amount of temperature rise, significant thermal effects would appear on the tissue surface, and the thermography method would be more effective in cancer detection.

It has been confirmed that the amount of temperature rise on the tissue surface depends on the tumor size and depth of location. In a study by Ng. et al. [38], a relationship was determined between the amount of heat generation and the tumor diameter. According to this study, the amount of heat generation by a tumor with the diameter of

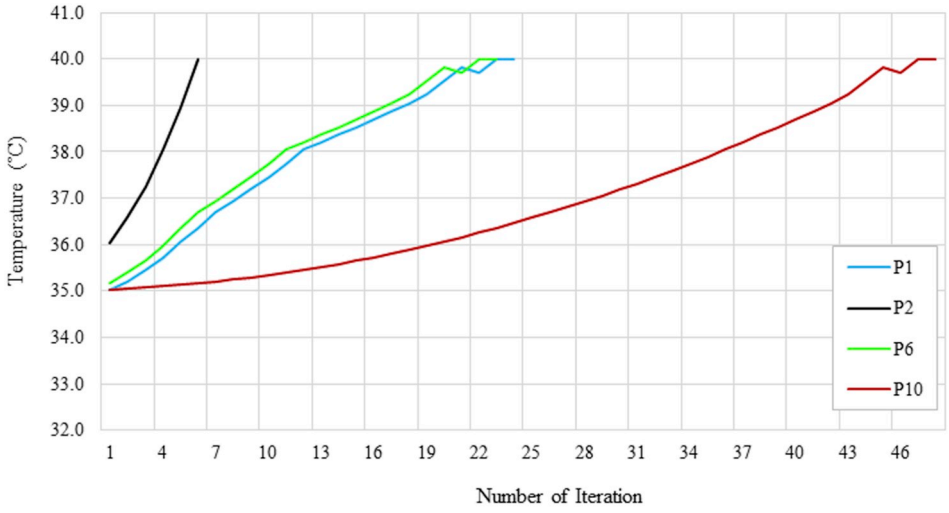

Fig. 13. The convergence plot to the maximum temperature in problems P_1, P_2, P_6 and P_{10} by one hunter on the 2D thermogram.

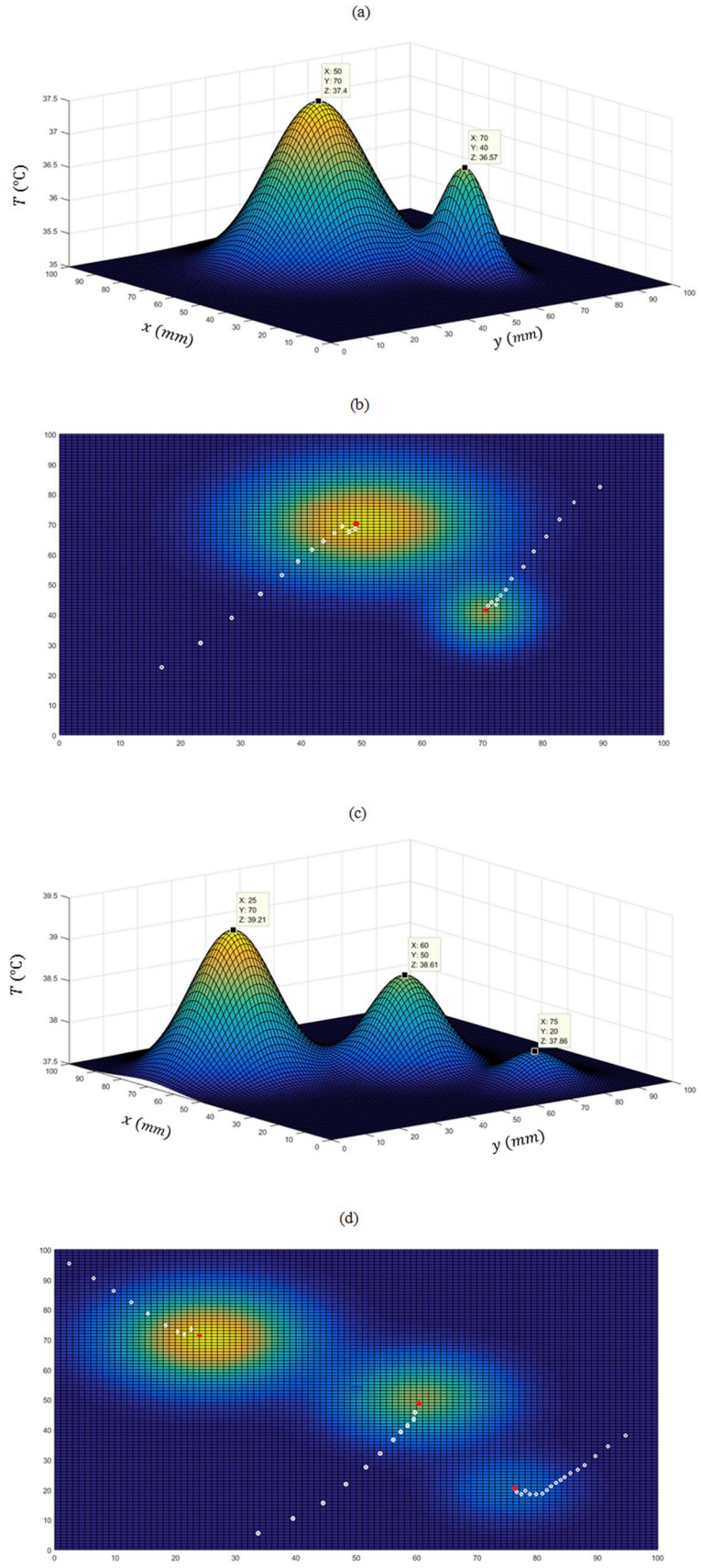

Fig. 14. The HA application to the tissue thermograms with multiple tumors.

Table 6
Parameters of the hunter algorithm for the application to thermograms of the breast tissue, the thermograms are obtained from Refs. [29,30], and each thermogram contains four tumors. Location and temperature values are scaled in the range of 0–100.

Thermograms [29,30]

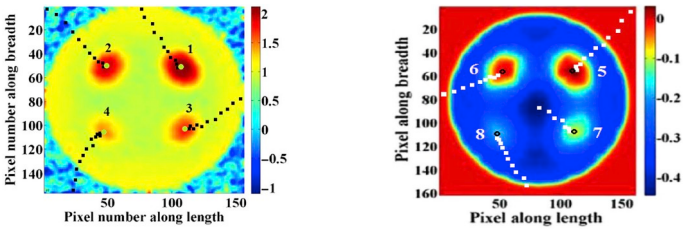

Tumor number			#1	#2	#3	#4	#5	#6	#7	#8
Number of iterations			12	12	12	13	12	10	8	13
Tumor parameters	Exact values	Location $0 < (x \& y) < 100$	(73,67)	(32,67)	(74,34)	(32,32)	(75,66)	(33,67)	(74,33)	(33,33)
		Temperature $0 < T < 100$	100	93	89	84	100	94	63	57
	Optimum values by HA	Location $0 < (x \& y) < 100$	(73,67)	(33,67)	(74,35)	(32,32)	(76,67)	(33,67)	(74,32)	(32,33)
		Temperature $0 < T < 100$	99.70	92.83	89.22	84.01	99.96	93.69	62.87	57.03

18 mm is about 10,000 $\frac{W}{m^3}$, while more heat is generated by larger tumors. The amount of heat generation by an 18 mm-diameter tumor increases the surface temperature up to 1 °C or 2.7%, which is not significant. Gorbach et al. [39] used an infrared camera and measured a temperature difference of 2.0 °C in the tumoral region compared to the healthy surrounding tissue. Keyserlingk et al. [40] showed that the smallest tumor diameter detectable by the thermography is 1.28 cm, which is smaller than the detectable size by conventional imaging methods. In this regards, small-sized tumors and deeply located tumors produce almost insignificant thermal effects on the tissue surface. For early tumor detection with a negligible temperature gradient, the Hunter algorithm could be employed. According to Fig. 14c and d, a 3 mm tumor with a temperature rise less than 1% or 0.3 °C, could be accurately detected by using the HA. In addition, the HA could reduce the inaccuracy of multiple tumor detection with more than one maximum temperature by employing a couple of hunters as the initial population. In this regard, the HA is applied to thermograms of the breast tissue obtained by Dua et al. [29] and Mulaveesala et al. [30] and it is observed that the tumors could be detected accurately. Moreover, the number of temperature measurement on the tissue surface is very limited which results in the reduction of the examination time.

At this stage, it is worth to mention that unlike most of the optimization and evolutionary algorithms such as the GA and the PSO, the performance of the HA is not disturbed by the determination of the number of the initial population. As it has been mentioned previously, unlike the evolutionary and swarm intelligence-based algorithms, the Hunter algorithm could be carried out by only one hunter as the initial population to find the prey. This is of particular importance in the tumor detection procedure by the contact thermography. In practice, use of one temperature sensor instead of multiple sensors (as the hunters) for scanning the tissue surface, would prevent the crosstalk effect on the measured values. Therefore, the accuracy of measurements is increased. As could be seen in Fig. 11a and b, the tumor is detected by one hunter on the thermogram.

5. Conclusions

In this paper, the thermography method is coupled with a novel optimization algorithm to rapidly detect and localize tumors inside the soft tissue. An examiner robot is used to construct a temperature map on the surface of tissue-mimicking phantoms. Study of this map provides data about the tumor existence and its location. This method has the privilege of being non-invasive to the body but has the disadvantage of being time-consuming to examine the entire tissue surface. To overcome this limitation, an optimization algorithm called the Hunter algorithm is proposed. Through this algorithm, the hunters approach the optimum value while few hunters are trapped in the local minima and a flock of hunters can hunt the prey. The effectiveness of the Hunter algorithm is tested by 11 mathematical test functions. Results show that the algorithm finds the global minima of these functions with a higher accuracy and faster than the GA and the PSO algorithm.

In addition to reducing the optimization costs, the novelty of the HA is the requirement to one hunter instead of a large number of the initial population. The Hunter algorithm with one hunter is used to find the maximum temperature on the thermograms obtained from 11 in vitro experiments. Results affirm that the Hunter algorithm can magnificently reduce the time required for identifying the location of maximum temperature. The time required to reach the deeply located tumors is increased, but it is still much less than the time required for examining the whole tissue surface. Moreover, the number of iterations depends on the initial location of the hunters on the hunting ground. Results illustrate that the rate of convergence is increased by getting closer to the prey at the initial state.

The HA has very important clinical application in the detection of small-sized and deeply located tumors with insignificant temperature gradient on the tissue surface. In addition, it is useful for the case of multiple tumors with several local maxima on the temperature map.

In conclusion, the thermography method in conjunction with the Hunter algorithm has various clinical applications in the tumor detection procedure. The proposed method could be employed as a screening tool for early detection of soft tissue tumors. Meanwhile, it is non-invasive to the body and less expensive compared to the conventional imaging techniques.

The authors are going to improve the method by performing experiments on human subjects. Moreover, they are extending the ability of the proposed method in the area of tumor features' extraction in their future study.

Funding

This research did not receive any specific grant from funding agencies in the public, commercial, or not-for-profit sectors.

Conflict of interest

The authors declare that they have no conflict of interest.

Ethical approval

This study does not involve human subjects.

Appendix A. Supplementary data

Supplementary data to this article can be found online at https://doi.org/10.1016/j.compbiomed.2019.103377.

References

[1] C.R. Gomez, Chapter 62 - disorders of body temperature, Handb. Clin. Neurol. 120 (2014) 947–957.

[2] S.G. Kandlikar, I. Perez-Raya, P.A. Raghupathi, J.L. Gonzalez-Hernandez, D. Dabydeen, L. Medeiros, P. Phatak, Infrared imaging technology for breast cancer detection – current status, protocols and new directions, Int. J. Heat Mass Transf. 108 (Part B) (2017) 2303–2320.

[3] P.R. Pavithra, K.S. Ravichandran, K.R. Sekar, R. Manikandan, The effect of thermography on breast cancer detection, Syst. Rev. Pharm. 9 (1) (2018) 10–16.

[4] R. Owen, S. Ramlakhan, R. Saatchi, D. Burke, Development of a high-resolution infrared thermographic imaging method as a diagnostic tool for acute undifferentiated limp in young children, Med. Biol. Eng. Comput. 56 (6) (2017) 1115–1125, https://doi.org/10.1007/s11517-017-1749-0.

[5] S. Matteoli, D. Coppini, A. Corvi, A novel image processing procedure for thermographic image analysis, Med. Biol. Eng. Comput. 56 (10) (2018) 1747–1756, https://doi.org/10.1007/s11517-018-1800-9.

[6] C. Magalhaes, R. Vardasca, J. Mendes, Recent use of medical infrared thermography in skin neoplasms, Skin Res. Technol. 00 (2018) 1–5 https://doi.org/10.1111/srt.12469.

[7] A. Bhowmik, R. Repaka, S.C. Mishra, Thermographic evaluation of early melanoma within the vascularized skin using combined non-Newtonian blood flow and bioheat models, Comput. Biol. Med. 53 (2014) 206–219.

[8] E. Sousa, R. Vardasca, S. Teixeira, A. Seixas, J. Mendes, A. Costa-Ferreira, A review on the application of medical infrared thermal imaging in hands, Infrared Phys. Technol. 85 (2017) 315–323 https://doi.org/10.1016/j.infrared.2017.07.020.

[9] A. Helmy, M. Holdmann, M. Rizkalla, Application of thermography for non-invasive diagnosis of thyroid gland disease, IEEE Trans. Biomed. Eng. 55 (2008) 1168–1175.

[10] S.V. Francis, M. Sasikala, Automatic detection of abnormal breast thermograms using asymmetry analysis of texture features, J. Med. Eng. Technol. 37 (1) (2013) 17–21.

[11] B. Kateb, V. Yamamoto, C. Yu, W. Grundfest, J.P. Gruen, Infrared thermal imaging: a review of the literature and case report, Neuroimage 47 (2009) T154–T162.

[12] S.V. Francis, M. Sasikala, G.B. Bharathi, S.D. Jaipurkar, Breast cancer detection in rotational thermography images using texture features, Infrared Phys. Technol. 67 (2014) 490–496.

[13] G. Shi, F. Han, C. Liang, L. Wang, K. Li, A novel method of thermal tomography tumor diagnosis and its clinical practice, Appl. Therm. Eng. 73 (1) (2014) 408–415.

[14] F. Bahramian, A. Mojra, Assessment of thermography technique for detection of thyroid gland: a numerical approach accompanied by an experimental study, Iranian Journal of Biomedical Engineering 10 (3) (2016) 245–256, https://doi.org/10.22041/ijbme.2017.72896.1268.

[15] M. Sadeghi-Goughari, A. Mojra, Intraoperative thermal imaging of brain tumors using a haptic thermal robot with application in minimally invasive neurosurgery, Appl. Therm. Eng. 91 (2015) 600e610.

[16] M. Sadeghi-Goughari, A. Mojra, Finite element modeling of haptic thermography: a novel approach for brain tumor detection during minimally invasive neurosurgery, J. Therm. Biol. 53 (2015) 53–65.

[17] M. Sadeghi-Goughari, A. Mojra, S. Sadeghi, Parameter estimation of brain tumors using intraoperative thermal imaging based on artificial tactile sensing in conjunction with artificial neural network, J. Phys. D Appl. Phys. 49 (2016) 075404.

[18] M. Mitchell, An Introduction to Genetic Algorithms, MIT Press, Cambridge, 1996.

[19] J. Kennedy, R. Eberhart, Particle swarm optimization, Proc. IEEE Int. Conf. Neural Netw. IV (1995) 1942–1948.

[20] - D. D. Karaboga, reportAn Idea Based on Honey Bee Swarm for Numerical Optimization, Technical Report-TR06, Erciyes University, Engineering Faculty, Computer Engineering Department.

[21] A. Colorni, M. Dorigo, V. Maniezzo, Distributed optimization by ant colonies, actes de la premiere conference europeenne sur la artificielle, Elsevier Publishing, Paris, France, 1991, pp. 134–142.

[22] V. Cerny, Thermodynamical approach to the traveling salesman problem: an efficient simulation algorithm, J. Optim. Theory Appl. 45 (1985) 41–51.

[23] R. Oftadeh, M. Mahjoob, M. Shariatpanahi, A novel meta-heuristic optimization algorithm inspired by group hunting of animals: hunting search, Comput. Math. Appl. 60 (2010) 2087–2098.

[24] K.F. Man, K.S. Tang, S. Kwong, Genetic algorithms: concepts and applications, IEEE Trans. Ind. Electron. 43 (5) (1996) 519–534.

[25] M. Mital, E.P. Scott, Thermal detection of embedded tumors using infrared imaging, J. Biomech. Eng. 129 (2007) 33–39.

[26] - T. Williams, Wanted: More Hunters, Audubon Magazine.

[27] - C.A. Harper, Quality Deer Management Guidelines for Implementation, Agricultural Extension Service, The University of Tennessee.

[28] E.P. Adorio, U.P. Diliman, MVF - multivariate test functions library in c for unconstrained global optimization, from, 2005. http://.wwwgeocities.ws/eadorio/mvf.pdf.

[29] G Dua, G.R Mulaveesala, Applicability of active infrared thermography for screening of the human breast: a numerical study, J. Biomed. Opt. 23 (3) (2018) 037001.

[30] R. Mulaveesala, G. Dua, Non- invasive and non-ionizing depth resolved infra-red imaging for detection and evaluation of breast cancer: a numerical study, Biomed. Phys. Eng. Expr. 2 (5) (2016) 055004.

[31] M. Mareli, B. Twala, An adaptive Cuckoo search algorithm for optimisation, Appl. Comput. Inf. 4 (2) (2018) 107–115.

[32] S.Hr Aghay Kaboli, J. Selvaraj, N.A. Rahim, Rain-fall optimization algorithm: a population based algorithm for solving constrained optimization problems, J. Comput. Sci. 19 (2017) 31–42.

[33] X.S. Yang, A new metaheuristic bat-inspired algorithm, in: J.R. González, D.A. Pelta, C. Cruz, G. Terrazas, N. Krasnogor (Eds.), Nature Inspired Cooperative Strategies for Optimization (NICSO 2010). Studies in Computational Intelligence, Springer, Berlin, Heidelberg, 2010, p. 284.

[34] X.S. Yang, Firefly algorithm, stochastic test functions and design optimization, Int. J. Bio-Inspired Comput. 2 (2010) 78–84.

[35] Emad Nabil, A modified flower pollination algorithm for global optimization, Expert Syst. Appl. 57 (2016) 192–203.

[36] T. Yu, L. Wang, X. Han, Y. Liu, L. Zhang, Swarm intelligence optimization algorithms and their application, WHICEB 2015 Proc. 3 (2015).

[37] S.V. Francis, M. Sasikala, Automatic detection of abnormal breast thermograms using asymmetry analysis of texture features, J. Med. Eng. Technol. 37 (1) (2013) 17–21.

[38] E.Y.K. Ng, N.M. Sudharsan, Numerical computation as a tool to aid thermographic interpretation, J. Med. Eng. Technol. 25 (2001) 53–60.

[39] A.M. Gorbach, J.D. Heiss, L. Kopylev, E.H. Oldfield, Intraoperative infrared imaging of brain tumors, J. Neurosurg. 101 (2004) 960.

[40] J.R. Keyserlingk, P.D. Ahlgren, E. Yu, N. Bellivean, Infrared imaging of breast: initial reappraisal using high-resolution digital technology in 100 successive cases of stage I and II breast cancer, Breast J. 4 (1998) 241–251.